International Journal of Microwave and Wireless Technologies, 2017, 9(7), 1499–1507. © Cambridge University Press and the European Microwave Association, 2017
doi:10.1017/S1759078717000083

RESEARCH PAPER

ISAR imaging of moving satellite based on GO–PO scattering model

JIAKUN WANG, MIN ZHANG, PENGBO WEI AND PANPAN JIANG

An efficient algorithm is proposed for the radar cross-section (RCS) prediction of complex target with electronically large size, which is a combination of geometrical optics and physical optics (GO–PO) method. The method taking the multiple reflections into account is applied to the electromagnetic scattering analysis of a satellite model. Then RCS curves of entire satellite model and the model without antenna structure are figured out. Based on the simulated echoes, the traditional inverse synthetic aperture radar (ISAR) images are discussed. Moreover, an application of motion compensation technique based on the joint time-frequency analysis is presented for ISAR imaging of the moving satellite that has both translational and rotational movements. Numerical results show good performance of GO–PO method in accuracy and efficiency and the great influence of the antenna with corner structures on the scattering characteristic of the satellite.

Keywords: GO–PO, EM scattering, ISAR imaging, Motion compensation, JTF

Received 26 October 2015; Revised 27 December 2016; Accepted 8 January 2017; first published online 10 February 2017

I. INTRODUCTION

Inverse synthetic aperture radar (ISAR) imaging of space target by simulating electromagnetic (EM) echoes provides a theoretical foundation to target classification, recognition, and so on. Although techniques for ISAR imaging have been fully developed, there still remain many problems owing to the particularity of the space target. In the simulation of radar echoes of a space target with particular structure such as corner reflector, the combination method of geometrical optics and physical optics (GO–PO) is proved to be an effective method. It is well suited for the EM scattering characteristics analysis of electrically large size targets [1, 2].

There exist several works to analyze the EM scattering characteristic from electrically large size targets with corner reflector structures. Knott [3] analyzed the radar cross-section (RCS) of dihedral corner reflections in the backward region using PO for single reflection and combination method for double reflection. Following a similar procedure, Ross [4] made an analysis of EM scattering characteristics of 90° dihedrals by considering edge diffraction effects. Anderson [5] also took higher order reflections into consideration and further investigated the effects of different dihedral angles on the EM scattering. Besides, Griesser [6] studied the backscattering of dihedral corner reflectors using both the GO–PO simplified method and more complicated PO-only technique over the entire azimuth plane. However, their works are only limited to the simple dihedral and trihedral corner reflectors.

School of Physics and Optoelectronic Engineering, Xidian University, Xi'an 710071, China
Corresponding author:
M. Zhang
Email: mzhang@mail.xidian.edu.cn

As for the low-frequency numerical methods, such as method of moments (MoM) [7] and multilevel fast multipole method (MLFMM) [8], the increase of electric size of target will notably aggravate the computational burden, $O(N^3)$ for MoM and $O(N^*[\log(N)]^2)$ for MLFMM, where N is the number of unknowns to be solved. However, the combination of GO–PO appears to be much more effective, especially for the high-frequency scattering prediction. The common simplification is to account for the initial reflection using GO whose advantage is that it can maintain the planar character of a wave upon reflection from a flat surface. The subsequent reflections are performed using PO. This allows us to estimate the EM scattering from electrically large and complex targets with high efficiency.

Since ISAR imaging of space target is able to provide motion parameters and structure features of the target [9], it is of great significance to develop a theoretical scattering model on ISAR imaging. A research on the theoretical and practical foundations of two-dimensional (2D) ISAR image collection and processing is made by Gombert and Beckner [10]. Yao and Zhou [11] simulated the ISAR imaging based on the scattering field calculated by the PO and ILDC (incremental length diffraction coefficient) methods. Zu *et al.* [12] investigated the broadband EM echoes via the GRECO (Graphical Electromagnetic Computing) technique and then obtained the ISAR images. Garcia-Fernandez *et al.* [13, 14] proposed a facet model of targets to study the ISAR images and back-scattering of moving targets with rigid and non-rigid motions. As for the ISAR imaging of moving target, there will be defocus and blur occurred in the images [15]. Various methods have been suggested to mitigate the unwanted motion effects in ISAR images, such as the entropy minimization method [16, 17], the joint time-frequency (JTF) methods [18, 19], and so on. Considering that most of previous works

https://doi.org/10.1017/S1759078717000083 Published online by Cambridge University Press

focus on the model consisting of ideal point scatterers, our attention is concentrated on the ISAR imaging simulation of a real moving target based on the scattered model.

The rest of this paper is structured as follows. Firstly, the principle of the combination of GO–PO method, which takes the multi-reflections into account, is described and followed by the theory of ISAR imaging of moving targets, including translational and rotational motions by utilizing the JTF method. Then, scattering characteristics of two satellite models, one of which is the entire model and the other without the antenna structure, are figured out and the comparison between simulated results and experimental results is given to validate the combination method. Besides, the conventional ISAR images of two satellite models based on the calculated scattering echoes are firstly simulated. Both of them show the great influence of the antenna with corner structures on the scattering characteristic of the satellite. Finally, the results of ISAR imaging of a moving satellite demonstrate the perfect compensation for the motion effects in imaging process.

II. GO-PO COMBINATION METHOD AND ISAR IMAGING

A) Principle of GO–PO

The basic idea of GO–PO to calculate a target's RCS is described in the following. First of all, the target model is approximated by small triangle patches whether illuminated or not. When incident EM wave illuminates a surface element, the reflection direction can be determined according to GO. Let the ray do the intersection test with patches which satisfy the condition $\hat{n}\cdot\hat{i}<0$, for that only these patches can possibly be illuminated by incident wave, where $\hat{i}$ is the unit vector of the incidence wave; $\hat{n}$ is the unit normal of the patch.

In this method, the square root of RCS consists of three components, described as [20]

$$\begin{aligned}\sqrt{\sigma}=&\sum\nolimits_0 i\frac{k}{\sqrt{\pi}}\int_{s_m}\hat{e}_r\cdot[\hat{s}\times(\hat{n}_m\times\hat{h}_i)]\exp(ik\vec{r}\cdot(\hat{i}-\hat{s}))ds_m\\&+\sum\nolimits_1 i\frac{k}{\sqrt{\pi}}\int_{s_m}\hat{e}_r\cdot[\hat{s}\times(\hat{n}_m\times\hat{h}_{r1m})]\\&\exp(ik\vec{r}\cdot(\hat{i}_{r1m}-\hat{s}))ds_m\\&+\sum\nolimits_2 i\frac{k}{\sqrt{\pi}}\int_{s_m}\hat{e}_r\cdot[\hat{s}\times(\hat{n}_m\times\hat{h}_{r2m})]\\&\exp(ik\vec{r}\cdot(\hat{i}_{r2m}-\hat{s}))ds_m,\end{aligned}\tag{1}$$

where the Σ_0, Σ_1, and Σ_2 are operated on the patches illuminated by the incident field, first reflected field, and second reflected field, respectively; $\hat{e}_r$ is the unit vector of electric polarization of far-field receiver; $\hat{s}$ is the unit vector of scattering wave; $\hat{n}_m$ is the unit normal of the m-th patch; $\hat{h}_i$ is a unit intensity vector of the incident magnetic field; $\hat{h}_{r1m}$ and $\hat{h}_{r2m}$ are the magnitude vectors of the first reflected and second reflected magnetic field illuminating on the m-th patch, respectively; $\hat{i}$ is the unit vector of incidence wave; $\hat{i}_{r1m}$ and $\hat{i}_{r2m}$ are the unit vectors along the direction of the first reflected and second reflected magnetic field illuminating on the m-th patch, respectively; s_m in the integral represents the surface of the m-th patch. Otherwise, the polygon integration over each patch can be easily converted into a contour integration with Gordon method. Take the m-th patch, for example [21]

$$\begin{aligned}&i\frac{k}{\sqrt{\pi}}\int_{s_m}\hat{e}_r\cdot[\hat{s}\times(\hat{n}_m\times\hat{h}_i)]e^{ik\vec{r}\cdot(\hat{i}-\hat{s})}ds_m\\&=\frac{\hat{e}_r\cdot[\hat{s}\times(\hat{n}_m\times\hat{h}_i)]}{\sqrt{\pi}T}e^{ik\vec{r}_o\cdot\vec{\omega}}\\&\quad\times\sum_{m=1}^{M}(\hat{p}\cdot\vec{a}_m)e^{ik\vec{r}_m\cdot\vec{\omega}}\frac{\sin(k\vec{a}_m\cdot\vec{\omega}/2)}{k\vec{a}_m\cdot\vec{\omega}/2},\end{aligned}\tag{2}$$

where $\vec{r}_o$ is the position vector of an origin on or near the patch; $\hat{p}=\hat{n}\times\vec{\omega}/\hat{n}\times\vec{\omega}$ is a unit vector in the plane of the patch perpendicular to $\vec{\omega}$, $\vec{\omega}=\hat{i}-\hat{s}$; T is the length of the projection of $\vec{\omega}$ onto the plane of the patch; $\vec{a}_m$ is a vector describing the length and orientation of the m-th edge of the patch, arranged tip to tail around the perimeter; $\vec{r}_m$ is the position vector of the midpoint of the m-th edge; and M is the number of patch edges.

Taking the dihedral corner reflector, for example firstly, it is assumed that if the central ray reflected by patch A intersects the patch B, the entire patch B is illuminated by parallel rays reflected by patch A. As Fig. 1 shows, the reflector is a right-angle corner and both surfaces have been partitioned into small triangle patches. Incident rays reflected by plate 1 intersect the plate 2 in some area. In Fig. 1(b), for $\theta_i<45^\circ$, the entire plate 2 is illuminated by the rays reflected from the bottom part of the plate 1. In this case, the number of the patches of the bottom part of the plate 1 is much less than that of the entire plate 2. If the normal central ray-tracing is still adopted, many patches of the plate 2 will be missed. For $\theta_i>45^\circ$, many patches of the plate 2 will be traced repeatedly.

Accordingly, the backward ray-tracing is adopted for the identification. For a patch on the plate 2, the tests with the patches, which have been illuminated by the incident rays, are done one by one. In every test, there is one patch A from plate 2 and one patch B from the illuminated patches of the plate 1. We let the origin of the ray be the direction contrary to the one of the ray reflected by patch B. If the ray and the patch B intersect with each other, it is considerate that the patch A is illuminated by the reflected field of the patch B. Otherwise, the test moves onto the next illuminated patch. If all the rays do not intersect the patches respectively, the patch A can be thought not illuminated by the reflected

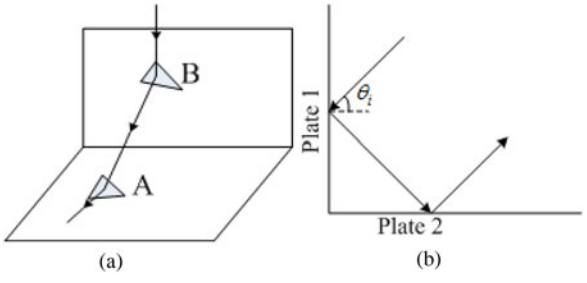


Fig. 1. General view of a ray illumination on a dihedral corner reflector. (a) Front view. (b) Lateral view.

https://doi.org/10.1017/S1759078717000083 Published online by Cambridge University Press

field. If the target structure is relatively complex, we must make sure that the ray is not cut by other patches between the patch A and patch B before the positive identification.

As for the computation about the second reflected field, the only thing need to do is to replace the patches illuminated by the incident wave by the ones illuminated by first reflected field, and the other parts of the algorithm are absolutely the same with the one for the first reflected field.

B) Verification of GO–PO algorithm

As we all know, the trihedral corner reflector is a typical benchmark target for the verification of high-frequency multiple-bounce scattering. The method above is applied to study the backscattering characteristic of a trihedral corner reflector, as is shown in Fig. 2, which is compared with MLFMM in FEKO as well as pure PO method for only first reflection considered. The trihedral corner reflector used in this paper is constructed of three right-angled triangles with the side length of 1 m.

The results show a great agreement between the combination method GO–PO result and the MLFMM result for both VV and HH polarizations at different frequencies, which proves the effectiveness and accuracy of the GO–PO method. The significant difference between GO–PO or MLFMM results and PO results indicates the dominant effect of multiple reflections on the scattering characteristic for such a corner reflector. The comparison of the computation time of two methods is illustrated in Table 1, which is the total time cost for all the 90 incidence angles. It is worth to notice that the GO–PO method appears to be much more efficient than MLFMM, especially in the high-frequency case.

III. ISAR IMAGING OF MOVING SATELLITE

ISAR generally refers to the case where the radar platform stays stationary while the target is moving. The motion of a target can be decomposed into the translational component and rotational component. It is assumed that there is a reference point usually located in the geometrical center of the target. The translational component refers to the movement of reference point along the track of moving target and the objective attitude relative to radar platform remains unchanged; the rotational component is that the target rotates around the reference point. When the target is represented by scatterers and is located in the far-field region of radar, the translational component has no influence on the radar echo Doppler. However, the translational component must be compensated in the imaging processing.

Assuming that the satellite moves along the radar line of sight (RLOS) axis, u, and rotates around its main axis, as Fig. 3 shows. The received signal can be theoretically approximated as an integration of the backscattered echoes from all scatterers inside the radar beam [18]

$$g(t) = \int\int_{-\infty}^{\infty} A(x, y) \exp\left(-j4\pi f \frac{r(t)}{c}\right) dxdy, \tag{3}$$

where $A(x, y)$ is the backscattered field amplitude of a point scatterer. For a target located at the far field relative to the radar, the distance from a point P to the radar can be expressed as

$$r(t) \cong R(t) + x\cos\varphi(t) - y\sin\varphi(t), \tag{4}$$

where $R(t)$ means the target's translational range off the radar and $\varphi(t)$ represents the rotational angle with respect to the RLOS. Then, the exponential term in equation (3) can be expanded into φ^t and φ^r that relate to the translational motion and the rotational motion, respectively.

$$\begin{aligned} \varphi^t &= \exp\left\{-j4\pi\frac{f}{c}\left(R_o + v_t t + \frac{1}{2}a_t t^2\right)\right\}, \\ \varphi^r &= \exp\left\{-j4\pi\frac{f}{c}[x_p\cos(\varphi_o + \omega_r t) - y_p\sin(\varphi_o + \omega_r t)]\right\}, \end{aligned} \tag{5}$$

where R_o is the initial position of the satellite; v_t and a_t are translational velocity and acceleration, respectively. φ_o is the initial angle and ω_r is the angular velocity of the satellite.

Considering the complicated target motions, the motion compensation (MOCOMP) technique must be applied to eliminate the undesired effects of motion on the ISAR

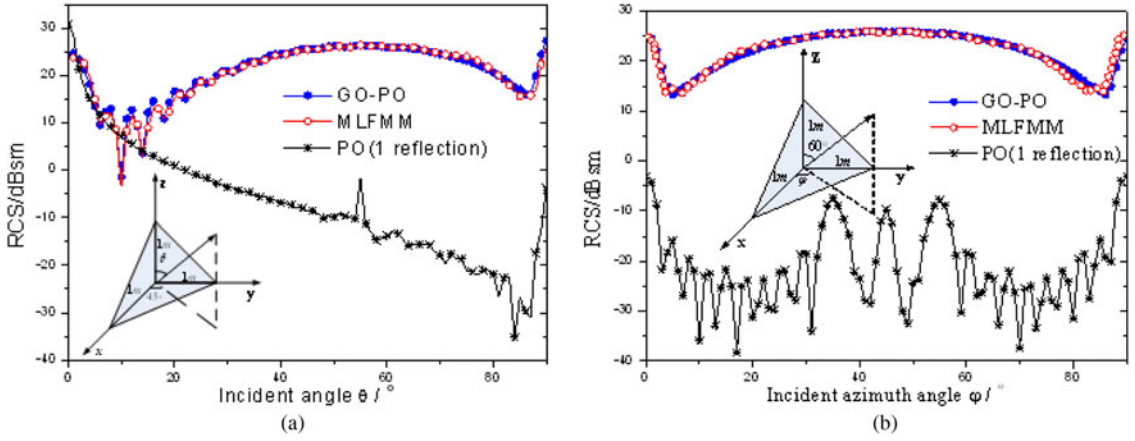


Fig. 2. Backscattering RCS comparison between GO–PO, MLFMM, and pure PO method for a trihedral corner reflector. (a) VV polarization for $\varphi = 45^\circ$ at 3.0 GHz. (b) HH polarization for $\theta = 60^\circ$ at 6.0 GHz.

https://doi.org/10.1017/S1759078717000083 Published online by Cambridge University Press

Table 1. Comparison of the computation time of different methods.

Method	MLFMM	GO–PO
Time for Fig. 2(a) (s)	1103	35.6
Time for Fig. 2(b) (s)	8174	68.4

image. Firstly, an estimation of the motion parameters is executed through the matching pursuit (MP) technique so as to compensate the radial motion errors [22–24]. The unknown translational motion parameters of v_t and a_t are estimated with an iterative search in a rough range of parameters by projecting the radar echoes on a 2D space. The estimated values v_t^{est} and a_t^{est} would be the parameters which give the largest projection

$$A = \max_{(v_t, a_t)}\{\langle g(t) \cdot \varphi^t(v_t, a_t, t)\rangle\}, \tag{6}$$

where the inner product is defined as

$$\langle g \cdot \varphi^t\rangle = \int_{v_t}\int_{a_t} g(t) \cdot (\varphi^t(v_t, a_t, t))^* da_t dv_t. \tag{7}$$

Then, the translational motion errors can be mitigated by a phase correction to the original echoes as follows

$$s(t) = g(t) \cdot \varphi^t(v_t^{est}, a_t^{est}, t)^*. \tag{8}$$

As for the rotational MOCOMP, the JTF transformation is applied to extract the instantaneous Doppler frequency information of the range-Doppler data so as to construct the snapshots of the time-varying ISAR image. The schematic algorithm is illustrated in Fig. 4. After translational MOCOMP to the scattered field, the 1D IFT (inverse Fourier transform) is firstly applied to obtain the range profiles. Based on this, an employment of JTF transformation is conducted to the pulses for every range cell, resulting in a time-range-Doppler cube of size $M \times N \times P$, which provides the range-Doppler image at a selected time instant. Finally, extraction of different slices from the cube corresponds to the instantaneous 2D ISAR image of the target while rotating.

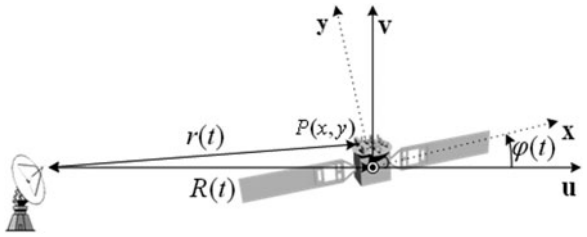


Fig. 3. Geometry of moving satellite with respect to radar.

IV. NUMERICAL RESULTS AND ANALYSIS

The GO–PO method is firstly used to analyze the EM scattering of a satellite model with complex antenna structures, which contains many corner structures, such as dihedral reflectors, as Fig. 5 shows. The model is 10.183 m long at the largest dimension and is partitioned into 46409 small patches. Here the model without antenna structure is partitioned into 31 084 small patches.

The comparisons of backscattering RCS results between the entire model and the model without antenna structure at 6.0 GHz for VV-polarization are shown in Fig. 6. In the following simulated results, the symbol N represents the model without antenna structure and E the entire satellite model. It can be seen obviously that the RCS for the complex satellite varies greatly with incident angle. The main reason is that the satellite model typically contains dozens of scatterers with significant contribution. The number of scatterers is so many that the contributions of all components to the RCS of the models are continuous either in phase or reverse phase, thus resulting in mutual interference, which leads to a heavy oscillation of the RCS curve. In Figs 6(a) and 6(b), it is illustrated that when in the XOZ plane, the entire antenna structure can be scanned in the range (0^o-90^o) of θ. Consequently, while removing the antenna structure, the RCS in the range (0^o-90^o) decreases about 20 dB. Moreover, for that the antenna cannot be illuminated in θ(90^o-180^o), the results of the two models show a slight difference. When in the XOY plane, as Fig. 6(c) shows, there are two peaks at 55° and 125° on the curve of the entire model for the multiple reflections, and both are about 20 dB larger than the RCS of the model without antenna. In the non-specific angles, as shown in Fig. 6(d), the RCS of entire satellite is larger than the other. Thus, the above analysis shows that the antenna structure is a strong scattering source. Furthermore, the multiple reflections among different structures and the corner reflectors could affect the scattering characteristic of a target greatly.

Figure 7 shows the comparison of GO–PO combination method result with the experimental result for RCS prediction

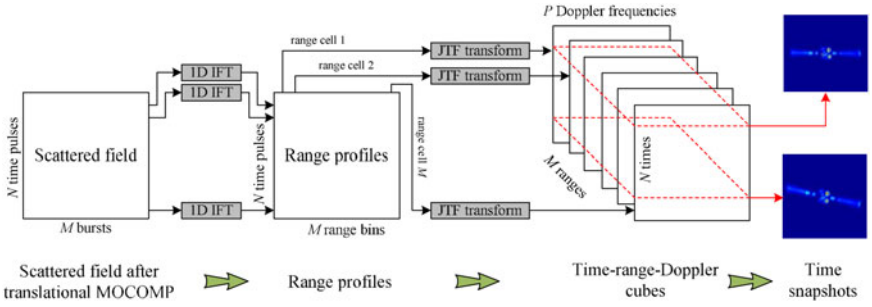


Fig. 4. Schematic representation of JTF method for the rotational MOCOMP.

https://doi.org/10.1017/S1759078717000083 Published online by Cambridge University Press

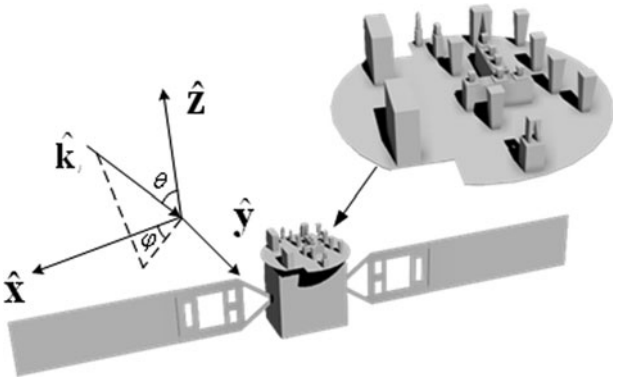


Fig. 5. Geometry of the satellite model.

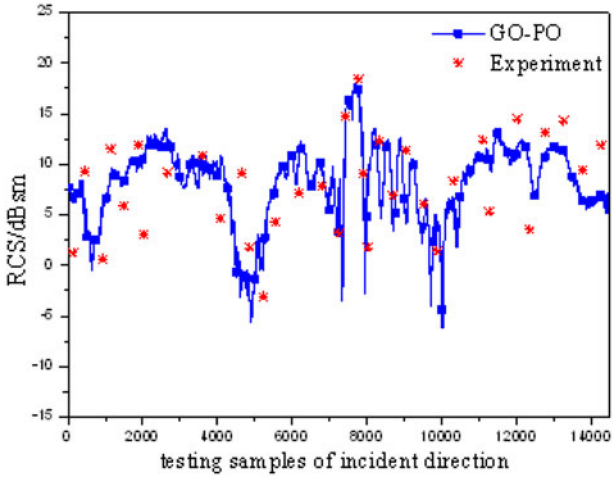


Fig. 7. Comparison of GO–PO result with experimental result for RCS prediction of satellite.

of the entire satellite model at 3.0 GHz for VV-polarization. Notably, both the incident angel θ and φ in simulation are consistent with the experimental process. The abscissa is only noted with sample numbers. From the contrast, the GO–PO method considering the multiple reflections appears a good agreement with the experiments. Therefore, this combination method is verified with enough accuracy for scattering analysis of such complex targets.

Since the simplicity and extensive application of range-Doppler method for ISAR imaging, it is first applied in the simple turntable model. In the simulations, the radar transmits stepped frequency signals at a central frequency 6.0 GHz with bandwidth 512 MHz, including $M = 128$ stepped frequencies in a burst and totally $N = 128$ bursts. The radar echoes are received from an incident angle $\theta = 45^{o}$ and an azimuth angle $\varphi = 45^{o}$. The ISAR imaging results are shown in Figs 8(a) and 8(b) for satellite with and without antenna structure, respectively. The comparison

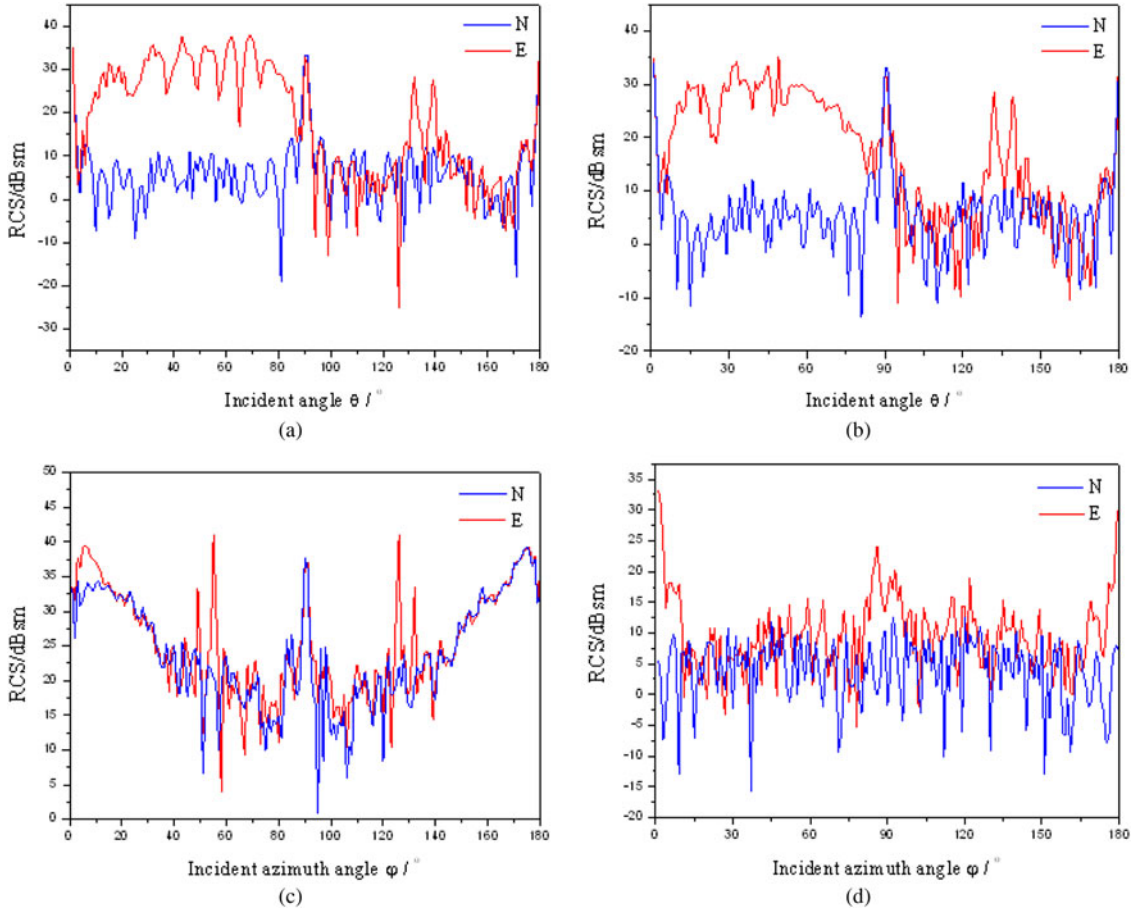


Fig. 6. Backscattering characteristics of satellite under different incident angle. (a) $\varphi = 0^{\circ}$. (b) $\varphi = 180^{\circ}$. (c) $\theta = 90^{\circ}$.(d) $\theta = 30^{\circ}$.

https://doi.org/10.1017/S1759078717000083 Published online by Cambridge University Press

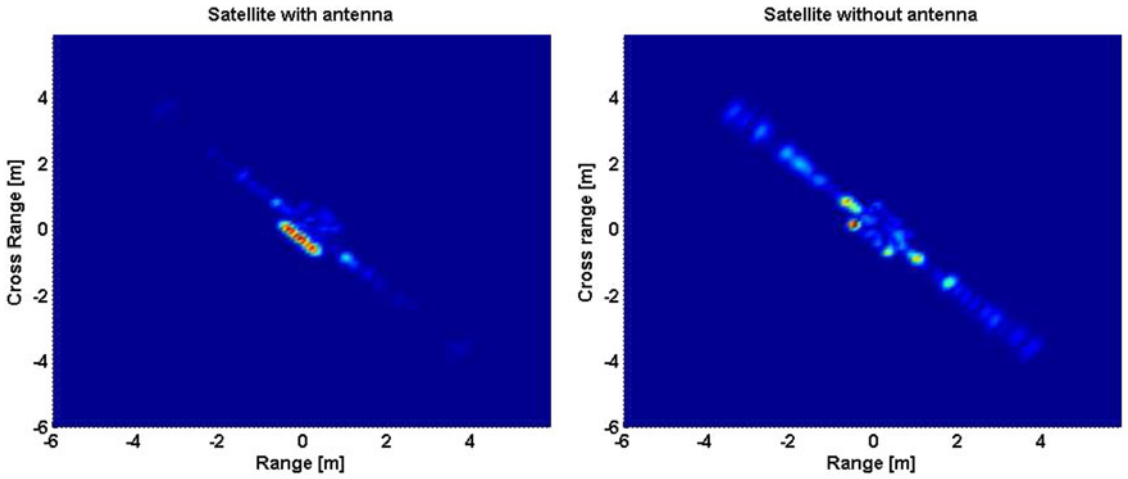


Fig. 8. ISAR images for the satellite models with and without antenna. (a) Satellite with antenna. (b) Satellite without antenna.

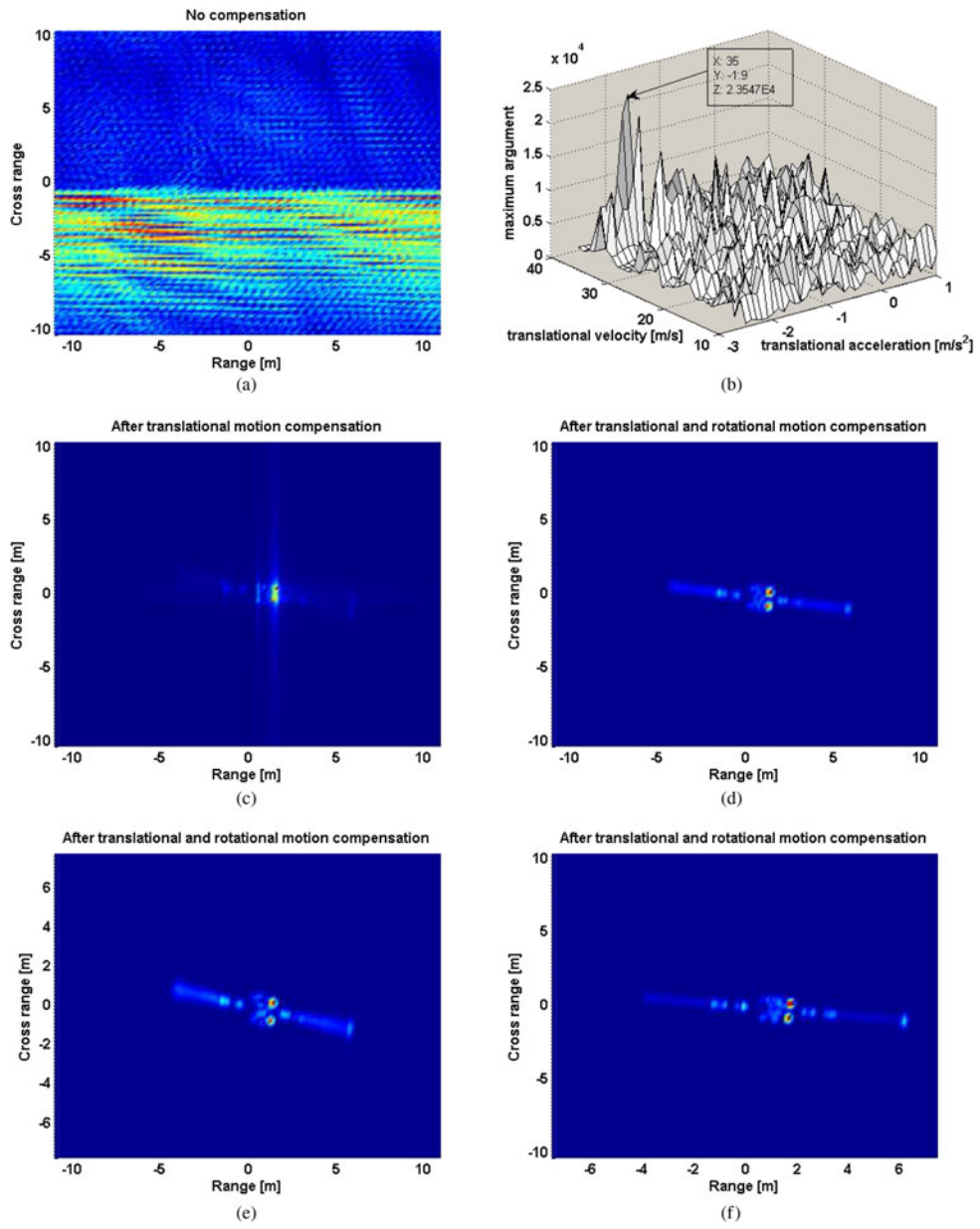


Fig. 9. ISAR images of moving satellite with antenna. (a) Conventional ISAR image (no compensation). (b) 2D MP search for translational parameters. (c) ISAR image (after translational MOCOMP). (d) ISAR image (after both MOCOMPs). (e) ISAR image (change angular velocity). (f) ISAR image (change bandwidth).

https://doi.org/10.1017/S1759078717000083 Published online by Cambridge University Press

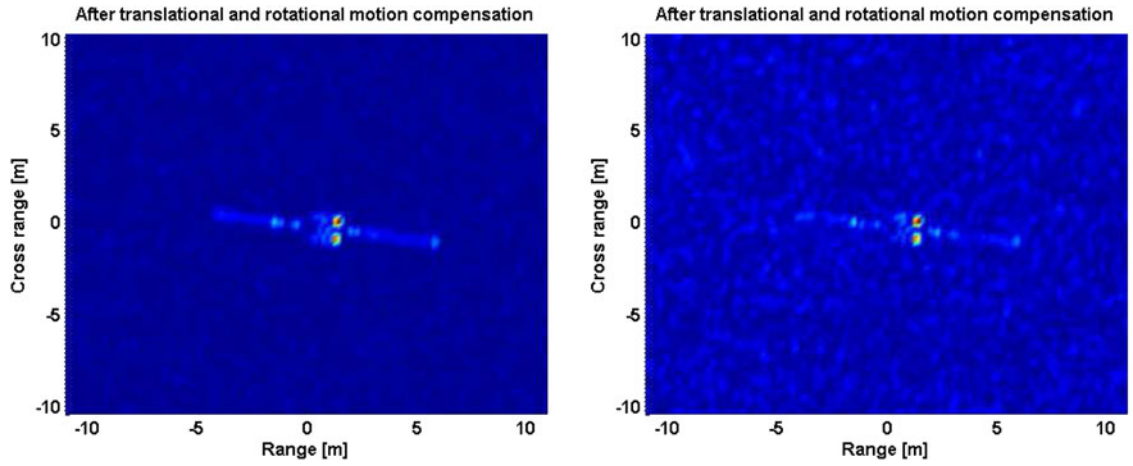


Fig. 10. ISAR images of moving satellite with additive random noise. (a) SNR = −10 dB. (b) SNR = −20 dB.

Table 2. Radar and target parameters for imaging simulation.

No. of pulses	128	No. of bursts	128
Initial velocity (m/s)	35.0	Radial acceleration (m/s²)	−1.9
Initial location (m)	1300	Initial azimuth (°)	0
Angular velocity (rad/s)	0.15	Central frequency (GHz)	3.0
Bandwidth (MHz)	864	Pulse repetition frequency (kHz)	8.0

between two images reflects that the antenna structure is almost the strongest scattering part and also weakens the effect of wing plate. This is owing to the fact that for a corner reflector, the maximum backscattering intensity always occurs near this incidence. However, the antenna on the satellite contains several reflectors, either dihedral or trihedral.

In the following simulations, assuming that the satellite with antenna has both translational and rotational movements, the motion parameters are listed in Table 2. The simulated results are shown in Fig. 9. However, without any compensation, see Fig. 9(a), the image is highly distorted, defocused, and blurred owing to high velocity in both radial and rotational directions. To compensate the translational motion, the MP search is used for the estimations of both translational velocity and acceleration. After the iterative search routine, the estimated values of $v_t^{est} = 35$ m/s and $a_t^{est} = -1.9$ m/s² are successfully found in Fig. 9(b). Accordingly, the translational MOCOMP can be executed by employing equation (8) and the corresponding ISAR image is plotted in Fig. 9(c). The image clearly demonstrates the performance of the translational MOCOMP so that only the rotational motion-based defocusing remains in the ISAR image. For the compensation of rotational motion effects, the Gabor-wavelet transform using Gaussian blur function is employed as the JTF tool. The resultant image is clearly given in Fig. 9(d), in which the phase errors caused by translational and rotational motions of the satellite have been eliminated. Therefore, the motion-free ISAR image is very well focused and the strong scattering centers are well localized on the antenna.

What's more, the ISAR images of the satellite under different parameters are simulated. Considering that the translational motion effects are always compensated based on the estimated values, the angular velocity and the bandwidth variations are realized for comparisons. Firstly, the angular velocity is increased to $\omega_r = 0.2$ rad/s with other parameters invariant and the result is shown in Fig. 9(e). With an increase of angular velocity, the total azimuth angle of the satellite rotates is larger than that in Fig. 9(d) in the same imaging integrated time, thus resulting in an improvement to the cross-range resolution. Meanwhile, the contribution of the wing plate to the received echoes is increased owing to the wider azimuth angle. In addition, change the bandwidth to $BW = 1264$ MHz and remain other parameters unchanged. The final ISAR image is illustrated in Fig. 9(f). The range resolution would be improved with the increasing signal bandwidth, thus the structure of satellite becomes clearer in range direction than in the Fig. 9(d).

To discuss the noise influence on ISAR images, Fig. 10 shows the ISAR images of moving satellite with additive random noise. The noise signal is chosen to be white Gaussian with the signal-to-noise ratio (SNR) of −10 and −20 dB. The simulation parameters keep the same as that in Fig. 9(d). Under a relative high SNR in Fig. 10(a), the scatterers on the satellite are resolved well in the motion-free ISAR image. While decreasing the SNR to −20 dB in Fig. 10(b), the wing plate structure would be a little harder to distinguish. However, the antenna structure is still easily observed owing to the strong radar scattering.

V. CONCLUSION

An efficient combination of GO and PO methods is proposed to study the EM scattering from electrically large and complex target with the consideration of multiple reflections. The model deals with the initial reflection using GO and the subsequent reflections are performed using PO. This could maintain the planar character of a wave upon reflection from a flat surface. In the ray-tracing part, the ray was traced backwards so that the contributions of some patches will not be missed or computed repeatedly. Numerical simulations are in excellent agreement with the measurements.

https://doi.org/10.1017/S1759078717000083 Published online by Cambridge University Press

In the ISAR imaging simulation of the moving complex satellite, the radar echoes are collected at different frequencies and positions. The proposed GO–PO method is shown to be much more effective than the low-frequency numerical method. By applying the MOCOMP technique, the imaging results prove that the multiple reflections from antenna structure are dominant in the EM scattering of the complex satellite. Besides, the strong noise shows greater influence on the wing plate than the antenna structure in the ISAR images.

ACKNOWLEDGEMENTS

This work was supported in part by the Fundamental Research Funds for the Central Universities, the National Nature Science Foundation of China under Grant no. 61372004/41306188, and the Foundation of Science and Technology on Electromagnetic Scattering Laboratory.

REFERENCES

[1] Ruan, Y.Z.: Hai Chen: Radar Cross Section, Electronic Industry Press, Beijing, 1988.

[2] Youssed, N.N.: Radar cross section of complex targets. Proc. IEEE, **77**, (1989), 722–734.

[3] Knott, E.F.: RCS reduction of dihedral corners. IEEE Trans. Antennas Propag., **25** (1977), 406–409.

[4] Ross, R.A.: Application of geometrical diffraction theory to reflex scattering centers, in IEEE Antennas and Propagation Society Int. Symp., vol. **6,** 1968, 94–99.

[5] Anderson, W.C.: Consequences of nonorthogonality on the scattering properties of dihedral reflectors. IEEE Trans. Antennas Propag., **35** (1987), 1154–1159.

[6] Griesser, T.: Backscatter Analysis of dihedral corner reflector using physical optics and the physical theory of diffraction. IEEE Trans. Antennas Propag., **35** (1987), 1137–1145.

[7] Harrington, R.F.: Field Computation by Moment Methods, McMillan, New York, 1968.

[8] Sertel, K.; Volakis, J.L.: Multilevel fast multipole method solution of volume integral equations using parametric geometry modeling. IEEE Trans. Antennas Propag., **52** (2004), 1686–1692.

[9] Ozdemir, C.: Inverse Synthetic Aperture Radar Imaging with MATLAB, John Wiley & Sons, Canada, 2012.

[10] Gombert, G.; Beckner, F.: High resolution 2-D ISAR image collection and processing. Proc. IEEE, **1** (1994), 371–377.

[11] Yao, H.Y.; Zhou, H.Y.: ISAR Imaging of Complex Targets Based on Electromagnetic Scattering Field, Metamaterials 2012 Int. Workshop, Nanjing, 2012.

[12] Zu, Y.Z.; Zhang, D.C.; Yin, Z.P.: Broadband Electromagnetic Scattering Echo Generation and its ISAR Imaging Simulation, in Int. Conf. Microwave and Millimeter Wave Technology, Nanjing, 2008.

[13] Garcia-Fernandez, A.F.; Yeste-Ojeda, O.A.; Grajal, J.: Facet model of moving targets for ISAR imaging and radar back-scattering simulation. IEEE Trans. Aerosp. Electron. Sys., **46** (2010), 1455–1467.

[14] Garcia-Fernandez, A.F.; Grajal, J.; Yeste-Ojeda, O.A.: Back-scattering of a helicopter with a millimeter-wave LFMCW radar. IEEE Trans. Aerosp. Electron. Sys., **49** (2013), 2781–2792.

[15] Wang, H.Q.; Grenier, D.; Delisle, G.Y.: Translational motion compensation in ISAR image processing. IEEE Trans. Image Proc., **4** (1995), 1561–1571.

[16] Wang, G.Y.; Bao, Z.: The Minimum Entropy Criterion of Range Alignment in ISAR Motion Compensation, in Proc. Conf. Radar '97, Edinburgh, 1997.

[17] Xi, L.; Guosui, L.; Ni, J.: Autofocusing of ISAR image based on entropy minimization. IEEE Trans. Aerosp. Electron. Sys., **35** (1999), 1240–1252.

[18] Chen, V.C.; Ling, H.: Time-Frequency Transforms for Radar Imaging and Signal Processing, Artech House, Norwood, 2002.

[19] Chen, V.C.; Qian, S.: Joint time-frequency transform for radar range-Doppler imaging. IEEE Trans. Aerosp. Electron. Sys., **34** (1998), 486–499.

[20] Wei, P.Bo.; Zhang, M.: GPU-based combination of GO and PO for electromagnetic scattering of satellite. IEEE Trans. Antennas Propag., **60** (2012), 5278–5285.

[21] Gorden, W.B.: Far field approximation of the Kirchhoff–Helmholtz representation of scattering fields. IEEE Trans. Antennas Propag., **23** (1975), 590–592.

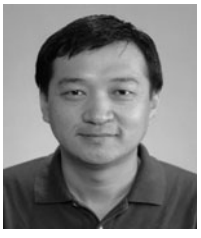
[22] Mallat, S.G.; Zhang, Z.: Matching pursuits with time-frequency dictionaries. IEEE Trans. Signal Process., **41** (1993), 3397–3415.

[23] Franaszczuk, P.J.; Bergey, G.K.; Durka, P.J.: Time-frequency analysis using the matching pursuit algorithm applied to seizures originating from the mesial temporal lobe. Electroencephalogr. Clin. Neurophysiol., **106** (1998), 513–521.

[24] Li, G.; Zhang, H.; Wang, X.; Xia, X.G.: ISAR imaging of maneuvering targets via matching pursuit, in IEEE Int. Geoscience and Remote Sensing Symp. (IGARSS), 2010, 1625–1628.



Jiakun Wang is with School of Physics and Optoelectronic Engineering, Xidian University, Xi'an 710071, China. His research interests include computational electromagnetic, ship hydrodynamics, and microwave remote sensing.



Min Zhang received the B.Sc. degree in Physics from Shaanxi Normal University, Xi'an, China, in 1990; the M.Sc. degree in Radio Physics from Xidian University, Xi'an, in 1998; and the Ph.D. degree in Astrometry and Celestial Mechanics from Shaanxi Astronomical Observatory, Chinese Academy of Sciences, Xi'an, in 2001. From 2001 to 2003, he was a Postdoctoral Research Fellow in Electromagnetic Field and Microwave Technique with Xidian University, where he is currently a Full Professor with the School of Science. From May 2003 to October 2004, he was a Research Fellow with the Department of Electrical and Computer Engineering, National University of Singapore, Singapore. His current research interests include electromagnetic model design, integral equation techniques, and fast hybrid algorithms for electromagnetic scattering, radiation, and wave propagation.

https://doi.org/10.1017/S1759078717000083 Published online by Cambridge University Press



Pengbo Wei was born in Shaanxi, China, in 1988. He received the Ph.D. degree in Radio Physics from Xidian University, Xi'an, China, in 2016. He is currently doing the post-doctoral research in School of Physics and Optoelectronic Engineering, Xidian University. His research interests include computational electromagnetics with application, theoretical, and statistical modeling on electromagnetic scattering from land and sea environments.



Panpan Jiang is with School of Physics and Optoelectronic Engineering, Xidian University, Xi'an 710071, China. Her research interests include computational electromagnetic, electromagnetic theory, and radar imaging.

https://doi.org/10.1017/S1759078717000083 Published online by Cambridge University Press